evaluation.[1,2] However, most of the paraboloidal reflectors produced at present have diameters of less than 5 m, and are measured by employing a time-consuming mechanical procedure using a template and gauge. It is therefore attractive to consider alternative methods which can maintain or improve accuracy and enable the measurement time to be reduced. A measurement scheme employing ultrasound has previously been suggested,[3] and is currently being examined in more detail.[4] The purpose of this letter is to propose and provide preliminary results of a microwave technique as a solution to the problem.

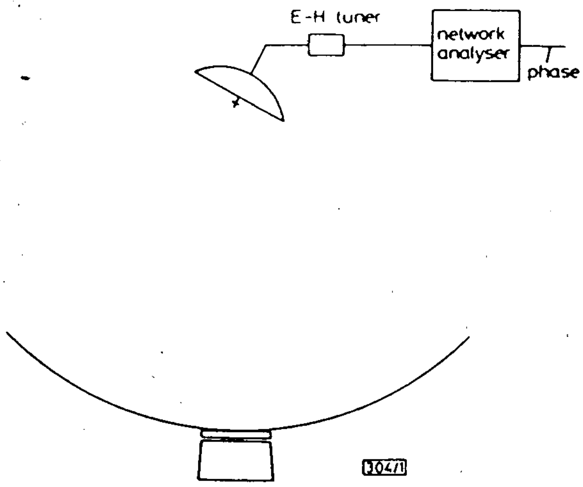

Fig. 1 *Reflector profiling system*

Fig. 1 shows the configuration of the profiling system. Here measurements are made at a single frequency by a small monostatic secondary reflector, located at the approximate centre of curvature of the paraboloid, which is around two focal lengths from the vertex. The small reflector is focused at the surface to be measured and, as the turntable rotates, variations in the transmit-receive path length are recorded as phase changes at the network analyser output. As will be seen later, such variations can be interpreted as profile deformations along an annular section of the antenna under test.

The choice of location for the secondary antenna is of particular importance, for it ensures that the wavefront from this antenna propagates close to the local normal to the large reflector. Therefore, after reflection, the majority of the wavefront is redirected to the secondary antenna as a well defined spherical phase front, and so helps to maximise the return signal level and hence the accuracy of the experiment.

The monostatic antenna must be carefully matched in order to avoid reflections which would perturb the phase of the signal received at the network analyser. For a phase accuracy of $\pm 1°$, the unwanted reflection must be maintained at least 35 dB below the signal received from the large reflector, and this was achieved in practice by suitable adjustment of the E-H tuner.

The spatial resolution of the system is governed by the footprint of the small antenna, and can be considered as the -3 dB width of the focused transmit-receive pattern. For the 45 cm-diameter reflector employed, a spatial resolution of 5 cm was achieved and the highest sidelobe of the composite response was -26 dB. The localised nature of the footprint is also beneficial in that tests need not be carried out in an anechoic environment. In fact, during the measurements described here, no precautions were taken with regard to the environment, and the small antenna was supported by a metal gantry which was also located in close proximity to the antenna under test.

In order to evaluate the capabilities of the method, a comparison technique was used to eliminate uncertainties concerning the profile of the reflector used. The antenna under test was of diameter 1·8 m and $f/D = 0{\cdot}3$. Measurements were made at a radius of 0·52 m and phase scans were recorded with and without the presence of known deformations in the form of small aluminium plates. A subtraction of successive scans was carried out to identify the nature of the added deformation.

Fig. 2 shows the result obtained for a configuration of three rectangular plates at an operating frequency of 9·85 GHz. The plates were distributed along the scan direction as shown in the Figure, and have the dimensions indicated. It can be seen from the plot that each deformation has been resolved clearly, and the table shows that the thickness of each plate has been measured to an accuracy of better than $\pm 0{\cdot}14$ mm. This result is very encouraging, in view of the fact that data sampling was carried out for convenience at equal time intervals and assumed a constant dish rotation speed. Evidence of the magnitude of error arising from this assumption is seen in the regions well away from the deformation, where variations as large as 3° ($\pm 0{\cdot}13$ mm) have occurred.

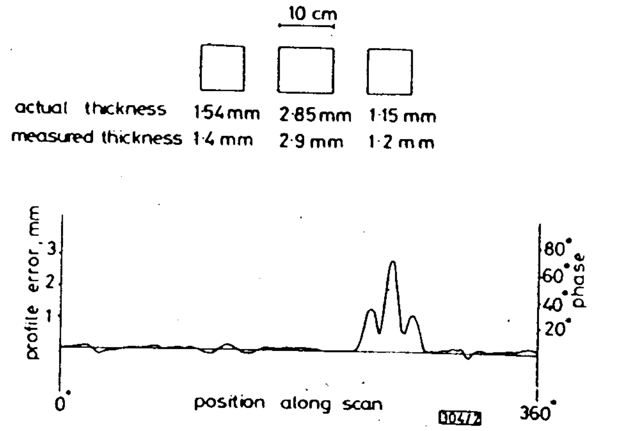

Fig. 2 *Configuration of deformations and results of profile measurement*

Inspection of surface annuli at other radii can in principle be achieved by mechanical rotation of the small antenna. Suitable compensation for the differential path length change with radius is carried out in arriving at the best-fit focal length for the reflector. However, to avoid mechanical scanning, a synthetic-aperture technique using a linear sampling array is currently under consideration, and allows all necessary data to be recorded from one revolution of the antenna under test.

J. C. BENNETT
D. G. SWAN

Department of Electronic & Electrical Engineering
University of Sheffield
Mappin Street, Sheffield S1 3JD, United Kingdom

3rd May 1985

References

1 BENNETT, J. C., ANDERSON, A. P., MCINNES, P. A., and WHITAKER, A. J. T.: 'Microwave holographic metrology of large reflector antennas', *IEEE Trans.*, 1976, **AP-24**, pp. 295–303

2 ANDERSON, A. P., BENNETT, J. C., WHITAKER, A. J. T., and GODWIN, M. P.: 'Measurement and optimisation of a large reflector antenna by microwave holography'. Proceedings of IEE international conference on antennas and propagation, London, November 1978, pp. 128–131

3 PARINI, C. G., and CLARRICOATS, P. J. B.: 'Reflector antenna profile measurement using ultrasound', *Electron Lett.*, 1980, **16**, pp. 544–546

4 PARINI, C. G., LAU, K. K., and CLARRICOATS, P. J. B.: 'Fast reflector profile tolerance measurement using ultrasound'. IEE colloquium on new developments and techniques in antenna measurements, Digest no. 1985/9, January 1985, pp. 7/1–4

POLARISATION ANALYSIS OF STRONGLY FUSED AND WEAKLY FUSED TAPERED COUPLERS

Indexing terms: Optical fibres, Optical connectors and couplers

The polarisation properties of both strongly fused and weakly fused single-mode tapered fibre couplers have been analysed. A comparison with experimental results shows excellent agreement with our analysis.

Introduction: Our recent understanding of the behaviour of tapers in single-mode fibres has allowed us to analyse in a very simple manner the behaviour of the fused tapered coupler.[1] In Reference 1 we studied the coupling behaviour of the well fused tapered coupler, while (and we quote the relevant results here) the coupling behaviour of the weakly fused coupler is equally straightforward to analyse. Both types are of interest, since in practice a fused coupler can be either well fused or weakly fused[2,3] (see Figs. 1a and b and Reference 3).

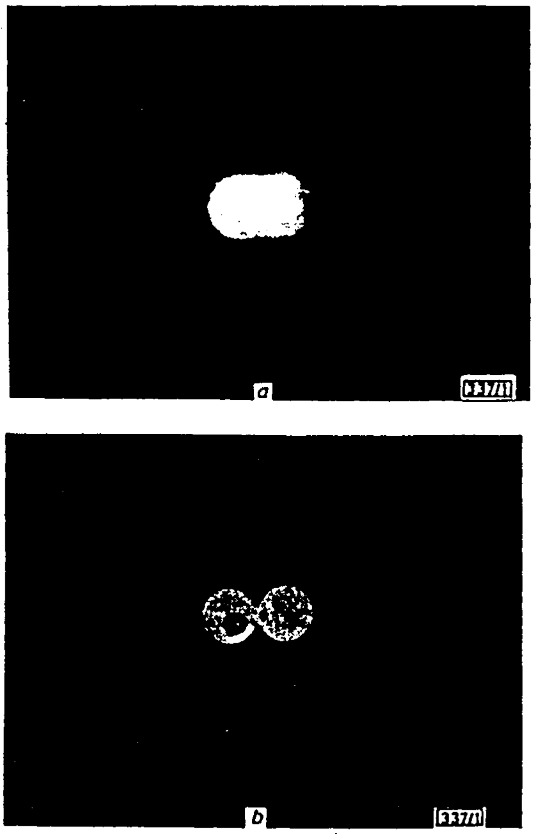

Fig. 1 *Photographs of cleaved cross-section of (a) strongly fused coupler and (b) weakly fused coupler*

Our main aim here is to show how the polarisation effects of both types of coupler can be accommodated within our overall model.

The polarisation behaviour of the fused coupler has been recently investigated experimentally,[4,5] and it has been shown that couplers with long interaction lengths can act as polarisation beam splitters. The behaviour of the power splitting ratio for unpolarised light as a function of wavelength for such couplers shows several characteristic features. The power splitting ratio oscillates rapidly as a function of wavelength with a channel spacing $\Delta\lambda$. This rapid oscillation is itself modulated with a slower period $\delta\lambda$, giving a response of a modulated comb filter.[4] The modulation arises as a result of the x- and y-polarisations having slightly different coupling strengths C_x and C_y in the fused section of the coupler. If the fused region is long enough, it is possible for complete dephasing between the two polarisations to occur, and one polarisation will exhibit complete power transfer at the output of the coupler. This will correspond to the observed nulls in the modulation period.[4]

Potentially, there are many applications which can exploit these properties of long couplers. They include polarisation beam splitters, spectral filters, modulators and switches. The successful design of such components requires a detailed knowledge of the coupling mechanisms within the coupler. In this letter we present the results of a detailed analysis of the coupling strengths of polarised light in both strongly and weakly fused couplers. We show that our analysis is in excellent agreement with recent measurements made on very long weakly fused couplers.[4]

Analysis: In Reference 1 we showed that the fused coupler can be successfully analysed by assuming that power exchanges occur as a result of the interference between the lowest-order symmetric and antisymmetric modes of the waveguide formed by the whole of the cross-section of the fused region. Typical dimensions of the fused region are 5 μm × 10 μm. The corresponding V-value is in the range 15–50, depending on whether the coupler is potted (potting index 1·42) or is in air. Such high V-values allow an accurate asymptotic analysis of the coupling strengths. The well fused guide is modelled by an equivalent rectangular guide (Fig. 2a) and the weakly fused coupler is modelled by two touching cylinders, corresponding to the fibre claddings (Fig. 2b). The fibre cores are of negligible cross-section in the fused taper and are ignored.

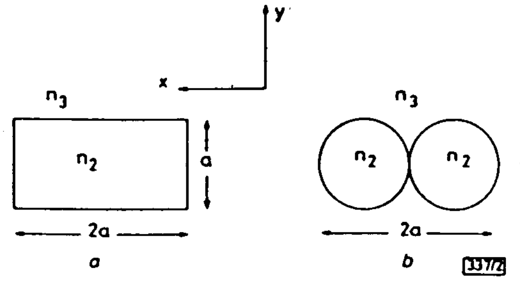

Fig. 2 *Model used to analyse coupling region of (a) strongly fused coupler and (b) weakly fused coupler*

If unpolarised light enters one of the input ports, then the power in an output port is described by

$$P = \tfrac{1}{2}[1 + \cos(C_x + C_y) \,.\, L \cos(C_x - C_y) \,.\, L] \tag{1}$$

where $C_{x,y}$ are the coupling strengths of the x- and y-polarisations and L is the length of the fused interaction region. To leading order in V the following equations for C_x and C_y have been derived:

(*a*) Strongly fused coupler:

$$C_x + C_y = \frac{3\pi\lambda}{32 n_2 a^2}\left[\frac{1}{\left(1 + \frac{1}{V}\right)^2} + \frac{1}{\left(1 + \frac{n_3^2}{n_2^2}\,\frac{1}{V}\right)^2}\right] \tag{2}$$

$$C_x - C_y = \frac{3\pi\lambda}{16 n_2 a^2} \cdot \frac{1}{V}\left(1 - \frac{n_3^2}{n_2^2}\right) \tag{3}$$

(*b*) Weakly fused coupler:

$$C_x + C_y = \frac{2^{7/2}(n_2^2 - n_3^2)^{1/2} U_\infty^2}{n_2 a \sqrt{(\pi)} V^{5/2}} \tag{4}$$

$$C_x - C_y = \frac{2^{5/2}(n_2^2 - n_3^2)^{1/2} U_\infty^2}{n_2^3 a \sqrt{(\pi)} V^{7/2}} \tag{5}$$

where $U_\infty = 2{\cdot}405$ and $V = [(2\pi a)/\lambda](n_2^2 - n_3^2)^{1/2}$.

These formulas allow the response of the coupler to be analysed for any input state of polarisation. They also display, in a very simple manner, the dependence on wavelength, refractive index and coupler size.

Discussion: From eqns. 2–5 it is straightforward to compute the channel spacing $\Delta\lambda$ and the modulation period $\delta\lambda$. The ratio of these two quantities has a particularly simple form, and is given by

$$\frac{\delta\lambda}{\Delta\lambda} = G \cdot \frac{V}{[1 - (n_3^2/n_2^2)]} \tag{6}$$

where $G = \frac{19}{14}$ for the weakly fused case and $\frac{1}{4}$ for the strongly fused case. Eqn. 6 predicts that the modulation period should decrease with increasing wavelength and that $\delta\lambda/\Delta\lambda$ should be proportional to 1/(wavelength). The experimental confirmation of this behaviour is contained in the measurements of very long fused couplers made in our laboratory, the results of which were presented in Reference 4. In Fig. 3 we have plotted $\delta\lambda/\Delta\lambda$ against $1/\lambda$ for one of these couplers with a 300 mm-long interaction region. The points lie close to a straight line, as predicted by eqn. 6. The fact that this graph does not pass through the origin is a consequence of our neglecting higher-order $1/V$ terms, which result in a constant being added to the right-hand side of eqn. 6. The cross-section of these couplers was examined by cleaving and photographing. Fig. 1*b* represents a typical result, and it is clear that these couplers were weakly fused. The gradient of a best straight-line fit to Fig. 3 allows the coupler cross-section to be determined using eqn. 6

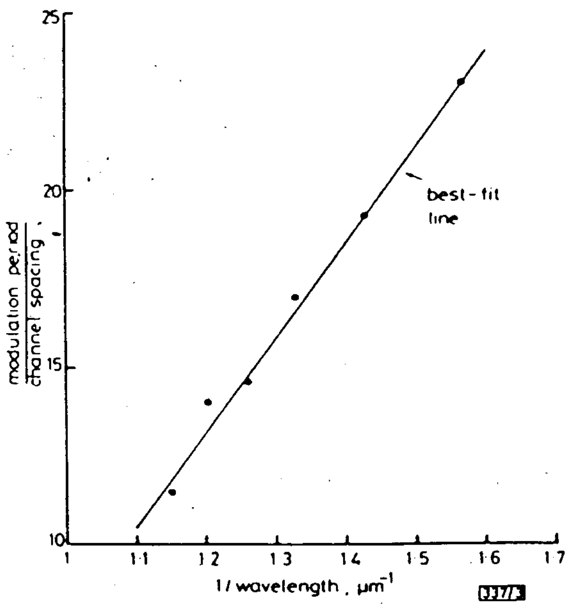

Fig. 3 *Experimental results for variation of modulation period/channel spacing against 1/(wavelength) for a weakly fused coupler with a 300 mm-long interaction region*

Experimental points are taken from previously reported measurements[4] performed at our laboratory

and G appropriate to the weakly fused case. We find that $a = 3\ \mu m$, in excellent agreement with the measured cross-section of our couplers.

In conclusion, we have presented the results of a detailed analysis of the coupling of x- and y-polarised light in strong and weakly fused couplers. Our results are in very good agreement with measurements made previously in weakly fused couplers.

Acknowledgment: The authors would like to thank Dr. D. N. Payne for helpful discussions and the UK SERC for financial support.

F. P. PAYNE
C. D. HUSSEY
M. S. YATAKI

13th May 1985

Department of Electronics & Information Engineering
The University
Southampton SO9 5NH, United Kingdom

References

1 PAYNE, F. P., HUSSEY, C. D., and YATAKI, M. S.: 'Modelling fused single-mode-fibre couplers', *Electron. Lett.*, 1985, **21**, pp. 461–462
2 LAMONT, R. G., JOHNSON, D. C., and HILL, K. O.: 'Power transfer in fused biconical-taper single-mode fiber couplers: dependence on external refractive index', *Appl. Opt.*, 1985, **24**, pp. 327–332
3 BRICHENO, T., and FIELDING, A.: 'Stable low-loss single-mode couplers', *Electron. Lett.*, 1984, **20**, pp. 230–232
4 YATAKI, M. S., PAYNE, D. N., and VARNHAM, M. P.: 'All-fibre wavelength filters using concatenated fused-taper couplers', *ibid.*, 1985, **21**, pp. 248–249
5 BRICHENO, T., and BAKER, V.: 'All-fibre polarisation splitter/combiner', *ibid.*, 1985, **21**, pp. 251–252

SIMPLE HYBRID MODE HORN FEED LOADED WITH A DIELECTRIC CONE

Indexing terms: Antennas, Horn antennas, Feeds, Dielectric, HE_{11} mode, Crosspolarisation

A conical horn loaded with a solid dielectric cone, separated from the metal wall by a thin layer of low-permittivity material or air, is analysed theoretically and tested experimentally. This simple feed exhibits excellent radiation properties, with a crosspolar bandwidth similar to that of a corrugated horn.

Introduction: Corrugated horns in different shapes are widely used as feeds in reflector antennas where low crosspolarisation is required. As these feeds are expensive to manufacture, there is a need for simpler and cheaper alternatives.

The investigations reported here and in Reference 1 were initiated by an interest in the low-permittivity dielectric cone feed studied extensively by P. J. B. Clarricoats and his coworkers.[2,3] To avoid dielectric foams, with their inherent problems caused by the softness of these materials and the difficulties in achieving perfect symmetry, it was decided to make some experiments with solid dielectrics.

During a study of the excitation of the solid cone, it was discovered that the proper condition for the balanced HE_{11}-mode to propagate could be achieved if the solid cone was surrounded by an outer thin layer of low-permittivity material and a metal wall, forming a rigid and simple construction, as shown in Fig. 1.

The front surface of the dielectric cone can be shaped by geometrical optics methods to control the phase distribution

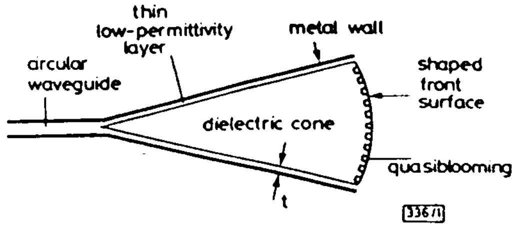

Fig. 1 *General geometry of horn antenna*

of the aperture field. For example, a plane wavefront can easily be obtained by an ellipsoidal front surface if a fixed-phase centre and minimum beamwidth are desired. Unwanted reflections from the front surface can be suppressed by a matching technique, drilling a number of approximately quarter-wavelength-deep and properly spaced holes in the surface.[4]

A similar type of horn is reported in Reference 5. This horn has an expanded dielectric cone with a rather low relative permittivity (1·13) and a plane front surface. The design formula for the thickness of the outer layer is valid only for cones with low permittivity. The advantages of the latter horn are low weight and low dielectric losses, and that there is no need for a matching layer at the front surface. The disadvantages are the need for a thicker outer layer, which results in a larger horn, and that there is no direct way of obtaining anything but spherical wavefronts in the aperture.

Thickness of low-permittivity layer: The balanced hybrid mode condition can be achieved by selecting a proper thickness of the low-permittivity layer. A simple but sufficiently accurate result can be derived from the plane-wave model of the boundary shown in Fig. 2. The balanced HE_{11}-mode can propagate in the dielectric cone if[6]

$$Z_\phi Z_z = \eta_1^2 \tag{1}$$

where $Z_\phi = E_\phi/H_z$ and $Z_z = -E_z/H_\phi$ are the surface impedances at the boundary between the dielectric cone and the outer layer, and η_1 is the intrinsic impedance of the cone material. If the plane-wave model is used, and if θ_1

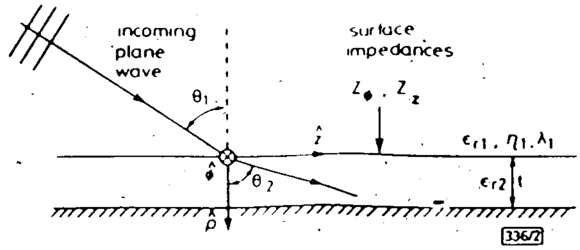

Fig. 2 *Simple plane-wave model to derive surface impedances*